

# Enhanced Data Detection for Massive MIMO with 1-Bit ADCs

Amin Radbord, Italo Atzeni, and Antti Tölli

Centre for Wireless Communications, University of Oulu, Finland

Emails: {amin.radbord, italo.atzeni, antti.tolli}@oulu.fi

**Abstract**—We present new insightful results on the uplink data detection for massive multiple-input multiple-output systems with 1-bit analog-to-digital converters. The expected values of the soft-estimated symbols (i.e., after the linear combining and prior to the data detection) have been recently characterized for multiple user equipments (UEs) and maximum ratio combining (MRC) receiver at the base station. In this paper, we first provide a numerical evaluation of the expected value of the soft-estimated symbols with zero-forcing (ZF) and minimum mean squared error (MMSE) receivers for a multi-UE setting with correlated Rayleigh fading. Then, we propose a joint data detection (JD) strategy, which exploits the interdependence among the soft-estimated symbols of the interfering UEs, along with its low-complexity variant. These strategies are compared with a naive approach that adapts the maximum-likelihood data detection to the 1-bit quantization. Numerical results show that ZF and MMSE provide considerable gains over MRC in terms of symbol error rate. Moreover, the proposed JD and its low-complexity variant provide a significant boost in comparison with the single-UE data detection.

**Index Terms**—1-bit ADCs, joint data detection, massive MIMO.

## I. INTRODUCTION

To leverage the wide bandwidths in the (sub-)THz spectrum, massive multiple-input multiple-output (MIMO) arrays are required at the transmitter and/or receiver to overcome the strong pathloss and penetration loss [1], [2]. In this respect, fully digital architectures are preferred to their hybrid analog-digital counterparts as they provide highly flexible beamforming and large-scale spatial multiplexing [3]. In this context, using low-resolution analog-to-digital/digital-to-analog converters (ADCs/DACs) is necessary to scale down the power consumption and complexity [4]–[6]. Remarkably, fully-digital architectures with few-bit or even 1-bit ADCs/DACs can outperform hybrid analog-digital ones in terms of both spectral and energy efficiency [7].

The data detection in massive MIMO systems with 1-bit ADCs has been the subject of many recent studies, e.g., [8]–[11]. In this paper, we extend our previous work [11], which characterized the expected values of the soft-estimated symbols (i.e., after the linear combining and prior to the data detection) for multiple user equipments (UEs) and with

maximum ratio combining (MRC) receiver at the base station (BS). Considering  $K$  UEs and a transmit constellation of  $L$  data symbols, the exhaustive single-UE data detection (SUD) method proposed in [11] maps each soft-estimated symbol of the target UE to one of the  $L^K$  expected values of the soft-estimated symbols based on the minimum distance criterion. This method has two main drawbacks: on the one hand, it performs an exhaustive search over the set of expected values of the soft-estimated symbols corresponding to the target UE resulting from all the possible data symbol vectors, whose size grows exponentially with the number of UEs; on the other hand, it does not take advantage of the interdependence among the soft-estimated symbols of the interfering UEs as it treats each UE individually. Moreover, the analysis in [11] is limited to the case of MRC, whereas more sophisticated linear receivers such as the zero-forcing (ZF) and minimum mean squared error (MMSE) receivers generally lead to better performance.

Considering the key observations above, we first provide a numerical evaluation of the expected values of the soft-estimated symbols when ZF and MMSE are adopted at the BS. Interestingly, these expected values can be obtained by simple scaling of their MRC counterparts, for which a closed-form expression was derived in [11]. Then, we propose new data detection strategies based on the minimum distance criterion with respect to the expected values of the soft-estimated symbols. We begin by introducing a naive approach based on the maximum-likelihood data detection adapted to the 1-bit quantization, which is referred to as quantized maximum likelihood (QML). This strategy, however, does not account for the additive white Gaussian noise (AWGN) needed for the proper scrambling of the 1-bit quantized signals at the different antennas. Then, we propose a joint data detection (JD) strategy that considers parallel data detection over all the UEs and exploits the interdependence among their soft-estimated symbols. Furthermore, we present a low-complexity variant of JD obtained by reducing the size of the search space. Numerical results show that ZF and MMSE provide substantial gains in terms of symbol error rate (SER) compared with MRC thanks to the reduced dispersion of the soft-estimated symbols around their expected values. In addition, the proposed JD and its low-complexity variant greatly outperform the exhaustive SUD described in [11] since the latter does not account for

This work was supported by the Research Council of Finland (336449 Profi6, 346208 6G Flagship, 348396 HIGH-6G, and 357504 EETCAMD) and by the European Commission (101095759 Hexa-X-II).

the interdependence among the soft-estimated symbols of the interfering UEs.

## II. SYSTEM MODEL

Let us consider a single-cell massive MIMO system where a BS equipped with  $M$  antennas serves  $K$  single-antenna UEs in the uplink. We use  $\mathbf{H} \triangleq [\mathbf{h}_1, \dots, \mathbf{h}_K] \in \mathbb{C}^{M \times K}$  to denote the uplink channel matrix, where  $\mathbf{h}_k$  represents the channel vector of UE  $k$ . Considering a general correlated Rayleigh fading channel model, we have  $\mathbf{h}_k \sim \mathcal{CN}(\mathbf{0}, \mathbf{C}_{\mathbf{h}_k})$ ,  $\forall k$ , where  $\mathbf{C}_{\mathbf{h}_k} \in \mathbb{C}^{M \times M}$  is the channel covariance matrix of UE  $k$ . Furthermore, we define  $\mathbf{h} \triangleq \text{vec}(\mathbf{H}) \in \mathbb{C}^{MK}$  and, accordingly, we have  $\mathbf{h} \sim \mathcal{CN}(\mathbf{0}, \mathbf{C}_{\mathbf{h}})$ , with  $\mathbf{C}_{\mathbf{h}} \triangleq \text{blkdiag}(\mathbf{C}_{\mathbf{h}_1}, \dots, \mathbf{C}_{\mathbf{h}_K}) \in \mathbb{C}^{MK \times MK}$ . For simplicity, and without loss of generality, we assume that all the UEs are subject to the same signal-to-noise ratio (SNR)  $\rho$  during both the channel estimation and the uplink data transmission (see, e.g., [5], [9]). Each BS antenna is connected to two 1-bit ADCs, one for the in-phase and one for the quadrature component of the received signal. In this context, we introduce the 1-bit quantization function  $Q(\cdot) : \mathbb{C}^{A \times B} \rightarrow \mathcal{Q}$ , with  $\mathcal{Q} \triangleq \sqrt{\frac{\rho K + 1}{2}} \{\pm 1 \pm j\}^{A \times B}$  and (see, e.g., [5], [9])

$$Q(\mathbf{X}) \triangleq \sqrt{\frac{\rho K + 1}{2}} (\text{sgn}(\text{Re}[\mathbf{X}]) + j \text{sgn}(\text{Im}[\mathbf{X}])). \quad (1)$$

### A. Channel Estimation

As in [4], we utilize the Busgang linear MMSE (BLMMSE) estimator to estimate the channels. Let  $\mathbf{P} \triangleq [\mathbf{p}_1, \dots, \mathbf{p}_K] \in \mathbb{C}^{\tau \times K}$  denote the pilot matrix, where  $\mathbf{p}_k \in \mathbb{C}^\tau$  represents the pilot vector for UE  $k$  and  $\tau$  is the pilot length. We assume  $\tau \geq K$  and orthogonal pilot vectors among the UEs. During the channel estimation, all the UEs simultaneously transmit their pilots and the signal received at the input of the ADCs at the BS is given by

$$\mathbf{Y}_p \triangleq \sqrt{\rho} \mathbf{H} \mathbf{P}^H + \mathbf{Z}_p \in \mathbb{C}^{M \times \tau} \quad (2)$$

where  $\mathbf{Z}_p \in \mathbb{C}^{M \times \tau}$  is the AWGN matrix with i.i.d.  $\mathcal{CN}(0, 1)$  elements. At this stage, we vectorize (2) as

$$\mathbf{y}_p \triangleq \text{vec}(\mathbf{Y}_p) \quad (3)$$

$$= \sqrt{\rho} \bar{\mathbf{P}}^* \mathbf{h} + \mathbf{z}_p \in \mathbb{C}^{M\tau} \quad (4)$$

with  $\bar{\mathbf{P}} \triangleq \mathbf{P} \otimes \mathbf{I}_M \in \mathbb{C}^{M\tau \times MK}$  and  $\mathbf{z}_p \triangleq \text{vec}(\mathbf{Z}_p) \in \mathbb{C}^{M\tau}$ . The BS observes the quantized signal

$$\mathbf{r}_p \triangleq Q(\mathbf{y}_p) \in \mathbb{C}^{M\tau} \quad (5)$$

and obtains the estimate of  $\mathbf{h}$  via the BLMMSE estimator as [4]

$$\hat{\mathbf{h}} \triangleq \sqrt{\rho} \mathbf{C}_{\mathbf{h}} \bar{\mathbf{P}}^T \mathbf{A}_p \mathbf{C}_{\mathbf{r}_p}^{-1} \mathbf{r}_p \in \mathbb{C}^{MK} \quad (6)$$

with

$$\mathbf{A}_p \triangleq \sqrt{\frac{2}{\pi}} (\rho K + 1) \text{Diag}(\mathbf{C}_{\mathbf{y}_p})^{-\frac{1}{2}} \in \mathbb{C}^{M\tau \times M\tau} \quad (7)$$

and  $\mathbf{C}_{\mathbf{r}_p} \triangleq \mathbb{E}[\mathbf{r}_p \mathbf{r}_p^H]$ . Finally, the estimate of  $\mathbf{H}$  is expressed as  $\hat{\mathbf{H}} \triangleq [\hat{\mathbf{h}}_1, \dots, \hat{\mathbf{h}}_K] \in \mathbb{C}^{M \times K}$ , with

$$\hat{\mathbf{h}}_k \triangleq \sqrt{\rho} \mathbf{C}_{\mathbf{h}_k} \bar{\mathbf{p}}_k^T \mathbf{A}_p \mathbf{C}_{\mathbf{r}_p}^{-1} \mathbf{r}_p \in \mathbb{C}^M \quad (8)$$

and  $\bar{\mathbf{p}}_k \triangleq \mathbf{p}_k \otimes \mathbf{I}_M \in \mathbb{C}^{M\tau \times M}$ .

### B. Data Detection

Let  $\mathbf{x} \triangleq [x_1, \dots, x_K]^T \in \mathbb{C}^K$  denote the data symbol vector comprising the data symbols transmitted by the UEs. We assume that  $\mathbf{x} \in \mathcal{S}^K$ , where  $\mathcal{S} \triangleq \{s_1, \dots, s_L\}$  represents the transmit constellation with  $L$  data symbols. During the uplink data transmission, all the UEs simultaneously transmit their data symbols and the signal received at the input of the ADCs at the BS is given by

$$\mathbf{y} \triangleq \sqrt{\rho} \mathbf{H} \mathbf{x} + \mathbf{z} \in \mathbb{C}^M \quad (9)$$

where  $\mathbf{z} \in \mathbb{C}^M$  is the AWGN vector with i.i.d.  $\mathcal{CN}(0, 1)$  elements. The BS observes the quantized signal

$$\mathbf{r} \triangleq Q(\mathbf{y}) \in \mathbb{C}^M \quad (10)$$

where we note that the scaling factor  $\sqrt{\frac{\rho K + 1}{2}}$  in (1) is such that the variance of  $\mathbf{r}$  coincides with that of  $\mathbf{y}$ . Then, the BS obtains a soft estimate of  $\mathbf{x}$  via linear combining as

$$\begin{aligned} \hat{\mathbf{x}} &\triangleq [\hat{x}_1, \dots, \hat{x}_K]^T \\ &= \mathbf{V}^H \mathbf{r} \in \mathbb{C}^K \end{aligned} \quad (11)$$

where  $\mathbf{V} \in \mathbb{C}^{M \times K}$  is the combining matrix based on imperfect channel estimation, which is carried out as described in Section II-A.

### Expected value of the soft-estimated symbols with MRC.

As in [11], let us assume that the MRC receiver is adopted at the BS. The combining matrix is given by  $\mathbf{V}^{(\text{MRC})} = \hat{\mathbf{H}}$  and the soft-estimated symbol of UE  $k$  can be expressed as  $\hat{x}_k^{(\text{MRC})} = \hat{\mathbf{h}}_k^H \mathbf{r}$  (cf. (12)), with  $\hat{\mathbf{h}}_k$  and  $\mathbf{r}$  given in (8) and (10), respectively. Then, the expected value of the soft-estimated symbol of UE  $k$  for a given data symbol vector  $\mathbf{x}$  is given by

$$\mathbf{E}_k^{(\text{MRC})} \triangleq \sqrt{\rho} \text{tr}(\mathbf{C}_{\mathbf{r}_p}^{-1} \mathbf{A}_p \bar{\mathbf{p}}_k^* \mathbf{C}_{\mathbf{h}_k} \mathbf{C}_{\mathbf{r}_p}) \quad (13)$$

with  $\mathbf{C}_{\mathbf{r}_p}$  introduced in Section II-A and where  $\mathbf{C}_{\mathbf{r}_p} \triangleq \mathbb{E}[\mathbf{r}_p \mathbf{r}_p^H]$  represents the cross-covariance matrix between the quantized signals received during the uplink data transmission and channel estimation. Note that  $\mathbf{C}_{\mathbf{r}_p}$  can be written in closed-form as in [11, Eq. (20)]. Considering  $K = 2$  and 16-QAM (quadrature amplitude modulation) data symbols, Fig. 1 shows the impact of the data symbol vector  $\mathbf{x}$  on the expected values of the soft-estimated symbols of UE 1. In particular, we observe that each of the  $L^2 = 256$  pairs of transmitted data symbols gives rise to a different expected value.

## III. ENHANCED DATA DETECTION

In this section, we first extend the analysis in [11], which is limited to the MRC receiver, by providing a numerical evaluation of the expected values of the soft-estimated symbols with ZF and MMSE. Then, we propose enhanced data detection strategies that account for the interdependence among the soft-estimated symbols of the interfering UEs.

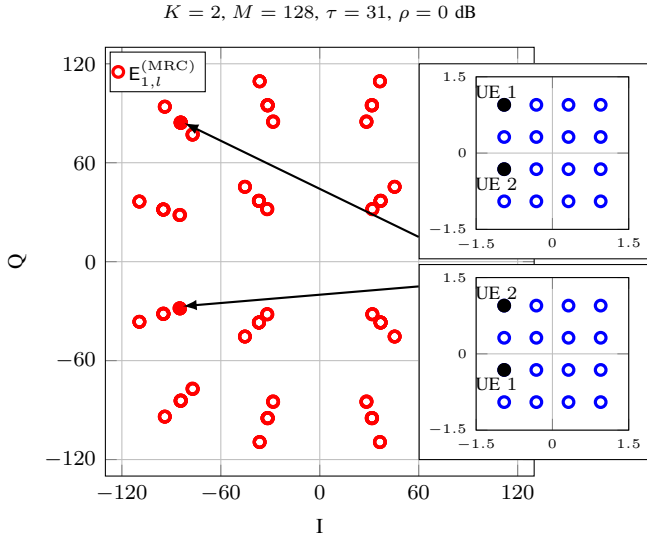


Fig. 1. Expected values of the soft-estimated symbols of UE 1 when UE 2 transmits all the possible data symbols from  $\mathcal{S}$ ; MRC is adopted at the BS.

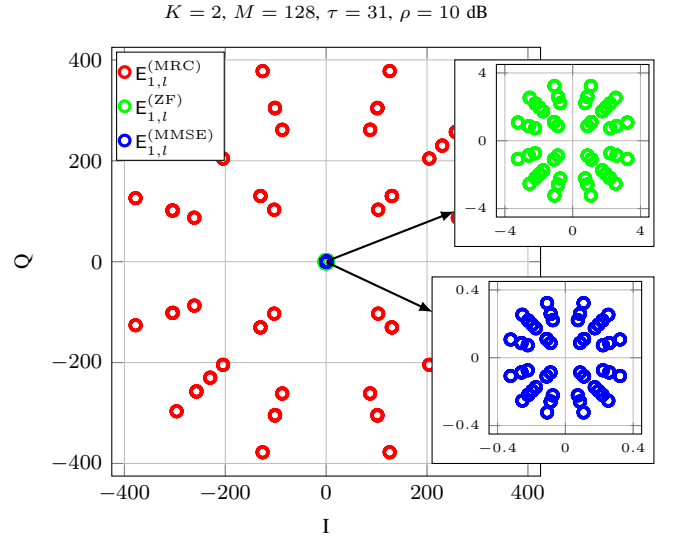


Fig. 2. Expected values of the soft-estimated symbols of UE 1 when UE 2 transmits all the possible data symbols from  $\mathcal{S}$ ; MRC, ZF, or MMSE is adopted at the BS.

#### A. Expected Value of the Soft-Estimated Symbols with ZF and MMSE

As done in Section II-B for MRC, we focus on the expected value of the soft-estimated symbols when ZF is adopted at the BS; the same steps can be followed for the MMSE receiver. The combining matrix is given by  $\mathbf{V}^{(ZF)} = \hat{\mathbf{H}}(\hat{\mathbf{H}}^H \hat{\mathbf{H}})^{-1}$  and the soft-estimated symbol for UE  $k$  can be expressed as  $\hat{x}_k^{(ZF)} = [(\hat{\mathbf{H}}^H \hat{\mathbf{H}})^{-1}]_{(k,:)} \hat{\mathbf{H}}^H \mathbf{r}$ . Then, the expected value of the soft-estimated symbol of UE  $k$  for a given data symbol vector  $\mathbf{x}$  is given by

$$\mathbf{E}_k^{(ZF)} \triangleq \mathbb{E}[\hat{x}_k^{(ZF)}] \quad (14)$$

where the expectation is taken over  $\mathbf{H}$ ,  $\mathbf{z}$ , and  $\mathbf{z}_p$ . Since the expected values of the soft-estimated symbols with ZF/MMSE are difficult to derive analytically, we use Monte Carlo simulations in this paper and leave the derivation of tractable expressions for future work. Considering  $K = 2$  and 16-QAM data symbols, Fig. 2 plots the expected values of the soft-estimated symbols of UE 1 corresponding to the three different linear receivers, i.e., MRC, ZF, and MMSE. Interestingly, we observe that the expected values with ZF/MMSE can be obtained by simple scaling of their MRC counterparts in (13). In this respect, let  $\alpha_k$  denote the scaling factor to be applied to the expected values with MRC so that they coincide with their counterparts obtained with ZF for UE  $k$ . Regarding the definitions in (13) and (14), let  $\mathbf{e}_k^{(MRC)}$  and  $\mathbf{e}_k^{(ZF)} \in \mathbb{C}^{L^K}$  denote the vectors containing all the possible expected values of the soft-estimated symbols for UE  $k$  with MRC and ZF, respectively. Then,  $\alpha_k$  can be computed as

$$\alpha_k \triangleq \underset{t > 0}{\operatorname{argmin}} \|\mathbf{e}_k^{(ZF)} - t \mathbf{e}_k^{(MRC)}\|. \quad (15)$$

Considering the same setup as in Fig. 2, Fig. 3 shows the above scaling factor of UE 1 versus the SNR assuming correlated and

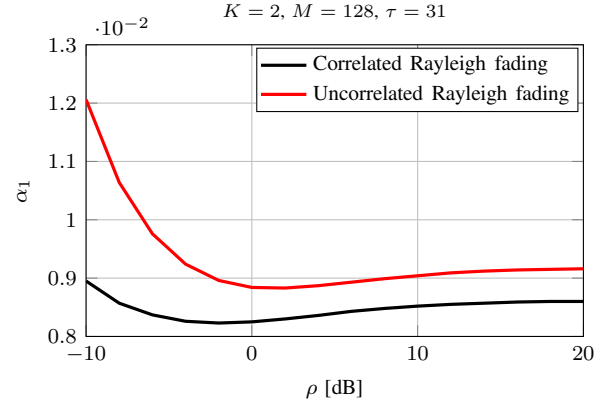


Fig. 3. Scaling factor between the expected values of the soft-estimated symbols of UE 1 obtained with MRC and ZF versus SNR; correlated and uncorrelated Rayleigh fading are considered.

uncorrelated Rayleigh fading channels, where the former are generated as described in Section IV. We observe that, with uncorrelated channels, the scaling factor exhibits a significant variation in the range of SNR values, whereas it appears more consistent in the case of correlated channels.

#### B. Data Detection Strategies

The exhaustive SUD proposed in [11] maps each soft-estimated symbol of the target UE to one of the  $L^K$  expected values of the soft-estimated symbols based on the minimum distance criterion. This method is impractical since it performs an exhaustive search over the set of expected values of the soft-estimated symbols corresponding to the target UE resulting from all the possible data symbol vectors, whose size grows exponentially with the number of UEs. In addition, it does not take advantage of the interdependence among the soft-estimated symbols of the interfering UEs as it treats each UE

individually. Hence, we present three data detection strategies that exploit this interdependence: 1) quantized maximum likelihood (QML), 2) joint data detection (JD), and 3)  $N$ -point joint data detection ( $N$ -JD). The QML represents a naive approach that adapts the well-known maximum-likelihood data detection to the 1-bit quantization. On the other hand, the JD and  $N$ -JD use the minimum distance criterion to map each soft-estimated symbol in (11) to one of the expected values of the soft-estimated symbols obtained as in (13) or (14) and, thus, to one of the possible data symbols in  $\mathcal{S}$ . In the following, we use  $l_k \in \{1, \dots, L\}$  and  $l_k^* \in \{1, \dots, L\}$  to denote the indices of the transmitted and detected data symbol for UE  $k$ , respectively.

1) *Quantized maximum likelihood (QML)*: This strategy detects the data symbol vector  $\mathbf{x}^*$  by simply finding the closest match between the quantized received signal  $\mathbf{r}$  and  $Q(\hat{\mathbf{H}}\mathbf{x})$  for all the possible data symbol vectors, i.e.,

$$\mathbf{x}^* = \underset{\mathbf{x} \in \mathcal{S}^K}{\operatorname{argmin}} \left\| \mathbf{r} - \sqrt{\rho} Q(\hat{\mathbf{H}}\mathbf{x}) \right\| \quad (16)$$

from which  $\{l_k^*\}_{k \in \mathcal{K}}$  can be extracted. We point out that comparing the noisy quantized received signal  $\mathbf{r}$  with  $Q(\hat{\mathbf{H}}\mathbf{x})$ , which neglects the AWGN altogether, is highly detrimental. In fact, a judicious amount of AWGN allows to effectively scramble the 1-bit quantized signals at the  $M$  antennas [9], [11] to recover the phase and amplitude of the transmitted data symbol. Instead, by overlooking the AWGN,  $Q(\hat{\mathbf{H}}\mathbf{x})$  yields identical values for all the elements of  $\hat{\mathbf{H}}\mathbf{x}$  falling into the same quadrant. Instead of examining the quantized received signal, it is more meaningful to consider the soft-estimated symbols obtained via linear combining, which embed the AWGN.

2) *Joint data detection (JD)*: This strategy takes the expected values of the soft-estimated symbols of the interfering UEs into account, which leads to enhanced data detection of the target UE. Regardless of which receiver is adopted at the BS, let  $\mathbf{E}_{k,l}(\mathbf{x}_{-k})$  denote the expected value of the soft-estimated symbol for UE  $k$  when  $x_k = s_l$  and the interfering UEs transmit  $\mathbf{x}_{-k} \triangleq [x_1, \dots, x_{k-1}, x_{k+1}, \dots, x_K]^T \in \mathbb{C}^{K-1}$ . For simplicity, and without loss of generality, we consider  $K = 2$  in the following. Let  $\mathbf{E}_{l,l'} \triangleq [\mathbf{E}_{1,l}(s_{l'}), \mathbf{E}_{2,l'}(s_l)]^T$  denote the vector containing the expected values of the soft-estimated symbols of the two UEs when  $x_1 = s_l$  and  $x_2 = s_{l'}$ . Let  $\mathcal{E} \triangleq \{\mathbf{E}_{l,l'}, \forall (s_l, s_{l'}) \in \mathcal{S}^2\}$  denote the set of vectors comprising the expected values of the soft-estimated symbols for both UEs resulting from all the possible data symbol vectors, with  $|\mathcal{E}| = L^2$ . The soft-estimated symbol vector  $\hat{\mathbf{x}}$  is mapped to one of the vectors  $\mathbf{E}_{l,l'} \in \mathcal{E}$  as

$$\mathbf{E}^* = \underset{\mathbf{E}_{l,l'} \in \mathcal{E}}{\operatorname{argmin}} \left\| \hat{\mathbf{x}} - \mathbf{E}_{l,l'} \right\| \quad (17)$$

from which  $\{l_k^*\}_{k \in \mathcal{K}}$  can be extracted. In general, this strategy amounts to performing an exhaustive search over all the  $L^K$  possible vectors  $\mathbf{E}_{l_1, \dots, l_K} \triangleq [\mathbf{E}_{1,l_1}(\mathbf{x}_{-1}), \dots, \mathbf{E}_{K,l_K}(\mathbf{x}_{-K})]^T$ . Hence, the complexity of this strategy increases exponentially with  $K$ .

3)  *$N$ -point joint data detection ( $N$ -JD)*: This strategy can be seen as a low-complexity variant of JD. Let  $\bar{\mathbf{E}}_{k,l} \triangleq \mathbb{E}_{\mathbf{x}_{-k}}[\mathbf{E}_{k,l}(\mathbf{x}_{-k})]$  represent the average of the expected values of the soft-estimated symbols of UE  $k$  when  $x_k = s_l$ . First, we consider the  $N \leq L$  values of  $\bar{\mathbf{E}}_{k,l}$  that are closest to each UE's soft-estimated symbol  $\hat{x}_k$ . In this regard, let  $\mathcal{S}'_k = \{s_{l_1}^{(k)}, s_{l_2}^{(k)}, \dots, s_{l_N}^{(k)}\}$  represent the set containing the detected symbols of UE  $k$ , where  $s_{l_i}^{(k)}$  denotes the detected symbol corresponding to the  $i$ th closest value of  $\bar{\mathbf{E}}_{k,l}$  to each soft-estimated symbol of UE  $k$ . Regarding  $\mathbf{E}_{l_1, \dots, l_K}$  defined in Section III-B2, let  $\mathcal{E}_{N\text{-JD}} \triangleq \{\mathbf{E}_{l_1, \dots, l_K}, \forall (s_{l_1}, \dots, s_{l_K}) \in \prod_{k=1}^K \mathcal{S}'_k\}$  denote the restricted set of vectors  $\mathbf{E}_{l_1, \dots, l_K}$  resulting from the data symbol vectors belonging to the Cartesian product of  $\mathcal{S}'_k$  across all the UEs, with  $|\mathcal{E}_{N\text{-JD}}| = N^K$ . The soft-estimated symbol vector  $\hat{\mathbf{x}}$  is mapped to one of the vectors  $\mathbf{E}_{l_1, \dots, l_K} \in \mathcal{E}_{N\text{-JD}}$  as

$$\mathbf{E}^* = \underset{\mathbf{E}_{l_1, \dots, l_K} \in \mathcal{E}_{N\text{-JD}}}{\operatorname{argmin}} \left\| \hat{\mathbf{x}} - \mathbf{E}_{l_1, \dots, l_K} \right\| \quad (18)$$

from which  $\{l_k^*\}_{k \in \mathcal{K}}$  can be extracted. As a result, the size of the search space is  $N^K$ , which can be made considerably smaller compared with  $L^K$  of JD by adjusting the value of  $N$ .

#### IV. NUMERICAL RESULTS

In this section, we evaluate the impact of the different receivers (i.e., MRC, ZF, and MMSE) and the data detection strategies described in Section III-B in terms of SER. We consider either  $K = 2$  or  $K = 3$  UEs, and unless otherwise stated, we assume that the BS is equipped with  $M = 128$  antennas. The set of data symbols  $\mathcal{S}$  corresponds to the 16-QAM constellation, i.e.,  $\mathcal{S} = \frac{1}{\sqrt{10}} \{ \pm 1 \pm j, \pm 1 \pm j3, \pm 3 \pm j, \pm 3 \pm j3 \}$ , which is normalized such that  $\frac{1}{L} \sum_{l=1}^L |s_l|^2 = 1$ . The channel covariance matrices are generated based on the one-ring channel model [12] with angular spread of  $30^\circ$  for each UE and angular separation of  $30^\circ$  between the UEs. All the UEs are subject to the same (normalized) pathloss, such that  $\operatorname{tr}(\mathbf{C}_{\mathbf{h}_k}) = M$ ,  $\forall k$ ; unless otherwise stated, we consider  $\rho = 0$  dB. The orthogonal pilots used for the channel estimation described in Section II-A are constructed as Zadoff-Chu sequences, which are widely adopted in the 4G LTE and 5G NR standards [13]; unless otherwise stated, we fix  $\tau = 31$ . All the SER results are obtained by averaging over  $4 \times 10^3$  independent channel and AWGN realizations and taking all the possible data symbols into account.

Considering  $K = 2$ , Fig. 4 plots the SER as a function of the SNR obtained with the data detection strategies described in Section III-B. For comparison, we also include the exhaustive SUD and the genie-aided data detection presented in [11]. As detailed in Section III-B, the exhaustive SUD does not take advantage of the interdependence among the soft-estimated symbols of the interfering UEs, whereas the genie-aided data detection assumes that the data symbols transmitted by the interfering UEs are perfectly known when detecting the symbols of the target UE. All the SER curves, except those corresponding to QML, feature an optimal SNR operating

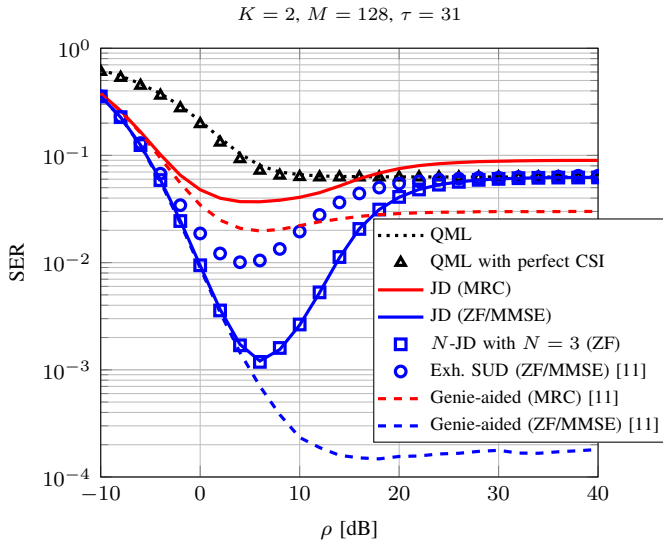


Fig. 4. SER versus SNR obtained with different data detection strategies and different receivers.

point: at low SNR, the AWGN is dominant; at high SNR, the soft-estimated symbols corresponding to the data symbols with the same phase are hardly distinguishable. In between these regimes, the right level of AWGN produces a proper scrambling of the 1-bit quantized signals at the  $M$  antennas. This phenomenon does not manifest with QML, where the SER decreases with the transmit SNR until it saturates. This is due to the fact that QML neglects the AWGN altogether, and its performance does not improve significantly even with perfect channel state information (CSI). However, the QML strategy outperforms JD with MRC at high SNR since the former seeks to pick up the best data symbol vector  $\mathbf{x}$  while the latter does not account for the interference among the different UEs. As demonstrated in Fig. 4, the genie-aided strategy outperforms JD for any receiver adopted at the BS. However, the genie-aided strategy cannot be implemented in practice and is considered only to evaluate how the knowledge of the data symbols transmitted by the interfering UEs impacts the data detection performance for the target UE. On the other hand, JD suffers from the error propagation between the detected symbols of the UEs, particularly at high SNR. Remarkably, there is a significant gain for all the data detection strategies obtained with the ZF and MMSE compared with their MRC counterparts. Here, the expected values of the soft-estimated symbols with the ZF/MMSE receivers are computed via Monte Carlo simulations. As demonstrated in Section III-A, these expected values can be obtained with simple scaling of the MRC counterparts in (13). As a result, the SER gain for the ZF/MMSE receivers is not due to their expected values but the reduced dispersion of the soft-estimated symbols around them. The exhaustive SUD method developed in [11] considers only the MRC receiver, but it can work with any receiver. In this regard, we have that JD and  $N$ -JD with  $N = 3$  provide a significant boost in comparison with the exhaustive SUD with

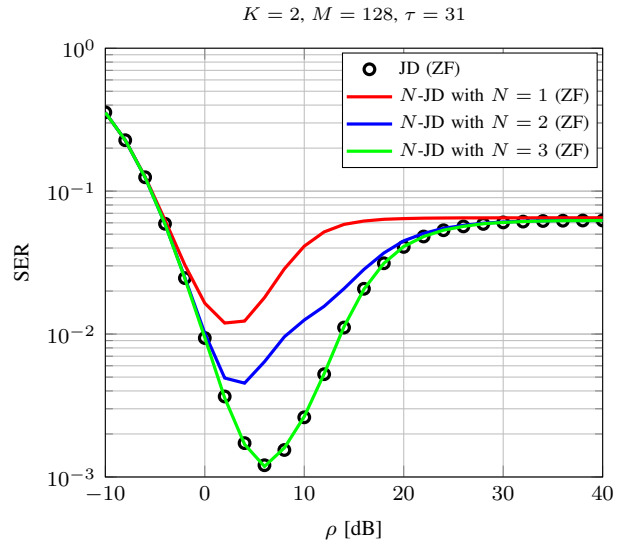


Fig. 5. SER versus SNR obtained with JD and  $N$ -JD (both with ZF).

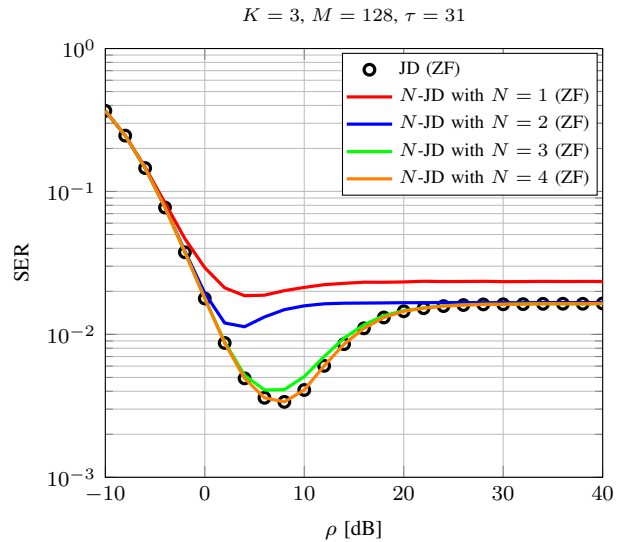


Fig. 6. SER versus SNR obtained with JD and  $N$ -JD (both with ZF).

the ZF/MMSE receivers. This means that taking advantage of the interdependence among the soft-estimated symbols of the interfering UEs gives a notable gain over the data detection strategies that treat each UE individually.

Considering again  $K = 2$ , Fig. 5 illustrates that  $N$ -JD exhibits the same performance with respect to JD with  $N = 3$ . This is because, with  $K = 2$ , there is significant overlap among many of the 256 expected values of the soft-estimated symbols. In addition, since there are three different amplitude levels in the 16-QAM constellation, only  $3 \times 16$  expected values can be clearly distinguished (see Fig. 1). Fig. 6 extends the insights of Fig. 5 to the case of  $K = 3$ . Here, there are  $16^3 = 4096$  different triplets of data symbols transmitted by the three UEs, each corresponding to a different expected value [11]. Remarkably,  $N$ -JD with  $N = 4$  perfectly matches

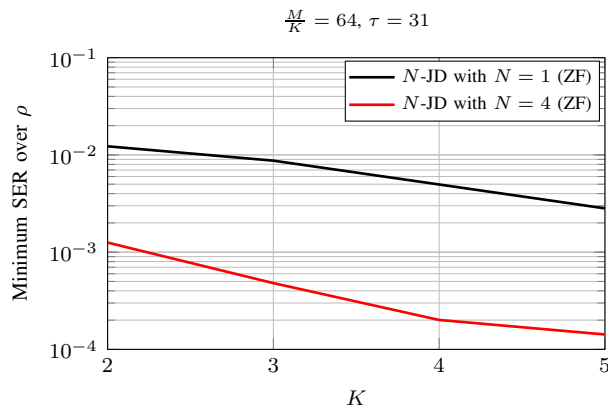


Fig. 7. Minimum SER over  $\rho$  versus number of UEs obtained with  $N$ -JD and ZF.

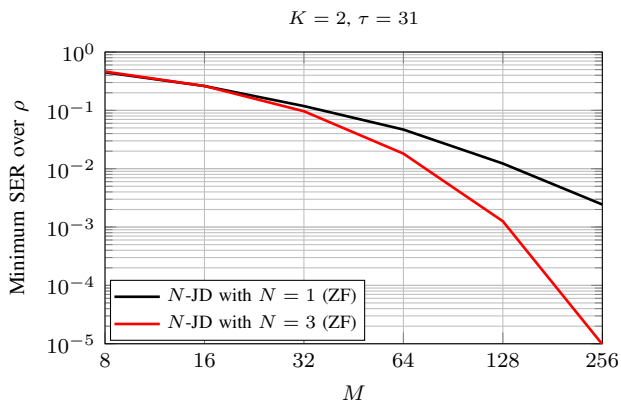


Fig. 8. Minimum SER over  $\rho$  versus number of BS antennas obtained with  $N$ -JD and ZF.

JD. This is because we have more distinguishable expected values with  $K = 3$  according to [11]. Therefore, we need to increase the size of the search space for  $N$ -JD to achieve the performance of JD perfectly.

Fig. 7 plots the minimum SER over the SNR  $\rho$  against the number of UEs for  $N$ -JD. It can be readily seen that the gap in Fig. 7 between  $N$ -JD with  $N = 4$  and  $N = 1$  does not change as  $K$  grows and the system load  $\frac{M}{K}$  remains fixed. This is because fixing  $\frac{M}{K}$  and increasing  $M$  and  $K$  lead to a higher beamforming gain, which better mitigates the impact of the interference among the different UEs. Considering  $K = 2$  and the data detection strategies depicted in Fig. 7, Fig. 8 illustrates the impact of the number of BS antennas  $M$  on the minimum achievable SER over the SNR  $\rho$ . We observe that the minimum SER monotonically decreases as  $M$  grows since higher granularity in the antenna domain contributes to a proper scrambling of a larger number of the 1-bit quantized signals.

## V. CONCLUSIONS

Considering a multi-UE setting with correlated Rayleigh fading, we investigated the uplink data detection in massive

MIMO system with 1-bit ADCs. In this study, we obtained the soft-estimated symbols for the ZF/MMSE receivers based on imperfectly estimated channels. Then, building on this result, we designed efficient data detection strategies based on the minimum distance criterion, which were compared in terms of SER and complexity. In this regard, we proposed a joint data detection strategy and its low-complexity variant, which take advantage of the interdependence among the soft-estimated symbols of the interfering UEs. Based on the numerical results, the proposed strategies with the ZF/MMSE receivers showed a significant gain in the SER compared with their counterparts with MRC, thanks to the reduced dispersion of the soft-estimated symbols around their expected values. Lastly, we demonstrated that increasing the number of UEs does not affect the SER gain in the proposed strategies over the exhaustive single-UE detection, provided that the system load is fixed.

## REFERENCES

- [1] N. Rajatheva, I. Atzeni, E. Björnson *et al.*, "White paper on broadband connectivity in 6G," <http://jultika.oulu.fi/files/isbn9789526226798.pdf>, 2020.
- [2] I. Atzeni, A. Tölli, D. H. N. Nguyen, and A. L. Swindlehurst, "Doubly 1-bit quantized massive MIMO," in *Proc. Asilomar Conf. Signals, Syst., and Comput. (ASILOMAR)*, 2023.
- [3] L. Lu, G. Y. Li, A. L. Swindlehurst, A. Ashikhmin, and R. Zhang, "An overview of massive MIMO: Benefits and challenges," *IEEE J. Sel. Topics Signal Process.*, vol. 8, no. 5, pp. 742–758, 2014.
- [4] Y. Li, C. Tao, G. Seco-Granados, A. Mezghani, A. L. Swindlehurst, and L. Liu, "Channel estimation and performance analysis of one-bit massive MIMO systems," *IEEE Trans. Signal Process.*, vol. 65, no. 15, pp. 4075–4089, 2017.
- [5] S. Jacobsson, G. Durisi, M. Coldrey, U. Gustavsson, and C. Studer, "Throughput analysis of massive MIMO uplink with low-resolution ADCs," *IEEE Trans. Wireless Commun.*, vol. 16, no. 6, pp. 1304–1309, 2017.
- [6] I. Atzeni, A. Tölli, and G. Durisi, "Low-resolution massive MIMO under hardware power consumption constraints," in *Proc. Asilomar Conf. Signals, Syst., and Comput. (ASILOMAR)*, 2021.
- [7] K. Roth, H. Pirzadeh, A. L. Swindlehurst, and J. Nosske, "A comparison of hybrid beamforming and digital beamforming with low-resolution ADCs for multiple users and imperfect CSI," *IEEE J. Sel. Topics Signal Process.*, vol. 12, no. 3, pp. 484–498, 2018.
- [8] J. Choi, J. Mo, and R. W. Heath, "Near maximum-likelihood detector and channel estimator for uplink multiuser massive MIMO systems with one-bit ADCs," *IEEE Trans. Wireless Commun.*, vol. 64, no. 5, pp. 2005–2018, 2016.
- [9] I. Atzeni and A. Tölli, "Channel estimation and data detection analysis of massive MIMO with 1-bit ADCs," *IEEE Trans. Wireless Commun.*, vol. 21, no. 6, pp. 3850–3867, 2022.
- [10] —, "Uplink data detection analysis of 1-bit quantized massive MIMO," in *Proc. IEEE Int. Workshop Signal Process. Adv. in Wireless Commun. (SPAWC)*, 2021.
- [11] A. Radbord, I. Atzeni, and A. Tölli, "Multi-user data detection in massive MIMO with 1-bit ADCs," in *Proc. IEEE Int. Conf. Acoust., Speech, and Signal Process. (ICASSP)*, 2023.
- [12] H. Yin, D. Gesbert, M. Filippou, and Y. Liu, "A coordinated approach to channel estimation in large-scale multiple-antenna systems," *IEEE J. Sel. Areas Commun.*, vol. 31, no. 2, pp. 264–273, 2013.
- [13] M. Hyder and K. Mahata, "Zadoff-Chu sequence design for random access initial uplink synchronization in LTE-like systems," *IEEE Trans. Wireless Commun.*, vol. 16, no. 1, pp. 503–511, 2017.